PHYSICS

Dominant nonlocal superconducting proximity effect due to electron-electron interaction in a ballistic double nanowire

Kento Ueda[1]*†, Sadashige Matsuo[1,2,3]*†, Hiroshi Kamata[1,2], Shoji Baba[1], Yosuke Sato[1], Yuusuke Takeshige[1], Kan Li[4], Sören Jeppesen[5], Lars Samuelson[5], Hongqi Xu[4,5,6]†, Seigo Tarucha[1,2]†

Cooper pair splitting (CPS) can induce nonlocal correlation between two normal conductors that are coupled to a superconductor. CPS in a double one-dimensional electron gas is an appropriate platform for extracting a large number of entangled electron pairs and is one of the key ingredients for engineering Majorana fermions with no magnetic field. In this study, we investigated CPS by using a Josephson junction of a gate-tunable ballistic InAs double nanowire. The measured switching current into the two nanowires is significantly larger than the sum of the switching current into the respective nanowires, indicating that interwire superconductivity is dominant compared with intrawire superconductivity. From its dependence on the number of propagating channels in the nanowires, the observed CPS is assigned to one-dimensional electron-electron interaction. Our results will pave the way for the utilization of one-dimensional electron-electron interaction to reveal the physics of high-efficiency CPS and to engineer Majorana fermions in double nanowire systems via CPS.

INTRODUCTION

The superconducting proximity effect can induce superconducting correlation in normal conductor nanostructures in contact with a superconductor. Therefore, it can provide a platform for engineering exotic phenomena and previously unidentified superconductivity. When two normal conductors are closely spaced, the proximity effect can inject nonlocal electron correlation between the two normal conductors, which is referred to as Cooper pair splitting (CPS) (*1*–*7*). CPS has been intensively studied in terms of generating nonlocally entangled spin pairs for applications in quantum information techniques. As a result, to date, CPS experiments have been exclusively performed on superconductors in contact with two quantum dots (*8*–*16*). In these devices, local pair tunneling (LPT), which occurs when two electrons in a single Cooper pair tunnel into the same dot, is strongly suppressed because of the large cost of electrostatic energy, and CPS can be dominant over LPT. To acquire a high-efficiency CPS-to-LPT ratio in the system, it is necessary to reduce the amount of dot to superconductor tunnel coupling and/or increase the electrostatic energy of the dots (*1*). However, in reality, this will also lead to a significant reduction of the conductance of the dots. Then, signals of CPS become tiny as the CPS-to-LPT ratio increases. Therefore, this way of engineering CPS is inappropriate for further experimental studies on the nature of split electrons (*17*).

One-dimensional (1D) electron gases can be considered as an alternative to quantum dots in the study of CPS because the 1D repulsive electron-electron (e-e) interaction is sporadically screened out (*18*, *19*), which can suppress LPT. Theoretically, the physics has already been developed for a hybrid system of two Tomonaga-Luttinger liquids (TLLs) contacting a superconductor (*5*). Unlike the case of quantum dots, CPS efficiency is only affected by 1D e-e interaction and not by the tunnel coupling of the 1D electron gas to the superconductors. This difference is crucial for extracting a large number of entangled spin pairs and holding nonlocal superconducting correlation into the double 1D electron gas. The former is useful for implementing efficient entangled spin pair sources in solid-state systems. For the latter, when the interwire proximity-induced superconductivity via CPS is dominant over the intrawire superconductivity via LPT in a parallel double nanowire (NW) (DNW), such as InAs or InSb, with strong spin-orbit interaction in terms of superconducting gap energy, the system is predicted to indicate time-reversal invariant topological superconductivity in which Kramers pairs of Majorana fermions (MFs) appear at the edges (*20*–*24*). Some signatures of topological superconductivity and MFs (*25*) have recently been reported in a single NW contacting a superconductor (*26*–*31*). However, in such a device, a strong magnetic field is required to realize the MFs, which can affect the robustness of MFs due to the quasiparticle (*32*). On the other hand, the proximity-induced superconductivity in the DNW can remove the restriction of a strong magnetic field and become a more robust platform for MFs and future topological quantum circuits. However, high-efficiency CPS and dominant interwire superconductivity have never been demonstrated via the CPS in 1D electron gases.

In this study, we report the first observation of CPS in a ballistic DNW Josephson junction based on the measurement of switching current. The CPS contribution in the switching current is dominant over the LPT contribution, which is ascribed to the 1D e-e interaction effects. In addition, Josephson junction devices enable us to evaluate the superconducting gap energies of the interwire and intrawire superconductivities as products of the switching current and normal resistance. We found that the gap of the interwire superconductivity is larger than that of the intrawire superconductivity, which is one of the necessary conditions to realize time-reversal invariant topological superconductivity and Kramers pairs of MFs. Our results will pave the way for the utilization of the 1D e-e interaction to reveal the physics of

[1]Department of Applied Physics, University of Tokyo, 7-3-1 Hongo, Bunkyo-ku, Tokyo 113-8656, Japan. [2]Center for Emergent Matter Science, RIKEN, 2-1 Hirosawa, Wako-shi, Saitama 351-0198, Japan. [3]JST, PRESTO, 4-1-8 Honcho, Kawaguchi-shi, Saitama 332-0012, Japan. [4]Beijing Key Laboratory of Quantum Devices, Key Laboratory for the Physics and Chemistry of Nanodevices and Department of Electronics, Peking University, Beijing 100871, China. [5]Division of Solid State Physics, Lund University, Box 118, SE-221 00 Lund, Sweden. [6]Beijing Academy of Quantum Information Sciences, Beijing 100193, China.
*These authors contributed equally to this work.
†Corresponding author. Email: kento.ueda@riken.jp (K.U.); sadashige.matsuo@riken.jp (S.M.); hqxu@pku.edu.cn (H.X.); tarucha@riken.jp (S.T.)

high-efficiency CPS and to engineer topological superconductivity and MFs in a DNW of not only InAs or InSb (*20*, *21*) but also chiral and helical edge states of topological insulators (*33*–*35*).

RESULTS

Normal conductance in a double InAs NW

The Josephson junction device used in this study has an InAs DNW between two Al electrodes with a small separation of 20 nm. A scanning electron microscope (SEM) image and schematic of the device are shown in Fig. 1 (A and B, respectively). The electron conductions of the two NWs are independently modulated using two separate gate electrodes labeled as g1 and g2 (orange). In this paper, we refer to the NW closest to g1 (g2) as NW1 (NW2).

First, we measured the differential conductance of the Josephson junction device at 50 mK under a larger magnetic field than the critical field for the Al electrode to characterize the normal transport property of the DNW (see note S2 and fig. S3). For the electron transport measurement, we used a standard lock-in technique. Figure 1C shows the measured differential conductance G as a function of the two voltages V_{g1} and V_{g2} for g1 and g2, respectively. The pinch-off regions for NW1 and NW2 are located below the blue solid line and to the left of the red solid line, respectively. The conduction can be divided into four regions separated by the red and blue solid lines: conduction of NW1 only (upper left), NW2 only (lower right), both NWs (DNW) (upper right), and no conduction (lower left).

Figure 1D shows the conductance line profiles related to Fig. 1C. The blue (red) lines indicate G of the only NW1 (NW2) measured by setting V_{g2} between −5.0 and − 8.0 V (V_{g1} between −17.0 and −20.0 V). For both conductance lines, we observe plateau-like structures characterized by the quantized conductance of $G = me^2/h$ with $m = 2, 4, 6$. The typical conductance data are shown by bold lines. Fluctuations of the conductance are likely due to impurity scattering, which depends on the two gate voltages. From the observation of the conductance plateau-like features, we confirm ballistic transport in each NW. Moreover, no definite tunnel junctions formed at the interface of the Al-NW junctions. In Fig. 1C, the dashed lines parallel to the blue or red solid lines or connecting the onsets of the respective conductance plateaus mark the transitions between neighboring plateaus in each NW. The conductance in each region bounded by two sets of neighboring dashed lines is then given by $G(m, n) = me^2/h + ne^2/h$, where m and n denote the number of propagating 1D channels in NW1 and NW2, respectively, and we call this region as (m, n).

Last, to characterize the electron transport in the DNW region, we show the conductance line profile along the thick purple line in Fig. 1C, as plotted in Fig. 1E. This purple line crosses (0,0) to (2,2) and to (4,4). Correspondingly, we observed conductance plateaus of 4 and 8 e^2/h. Hence, we confirmed that DNWs are ballistic, and the conductance in the normal state can be understood as the sum of the conductance values in the separate NWs.

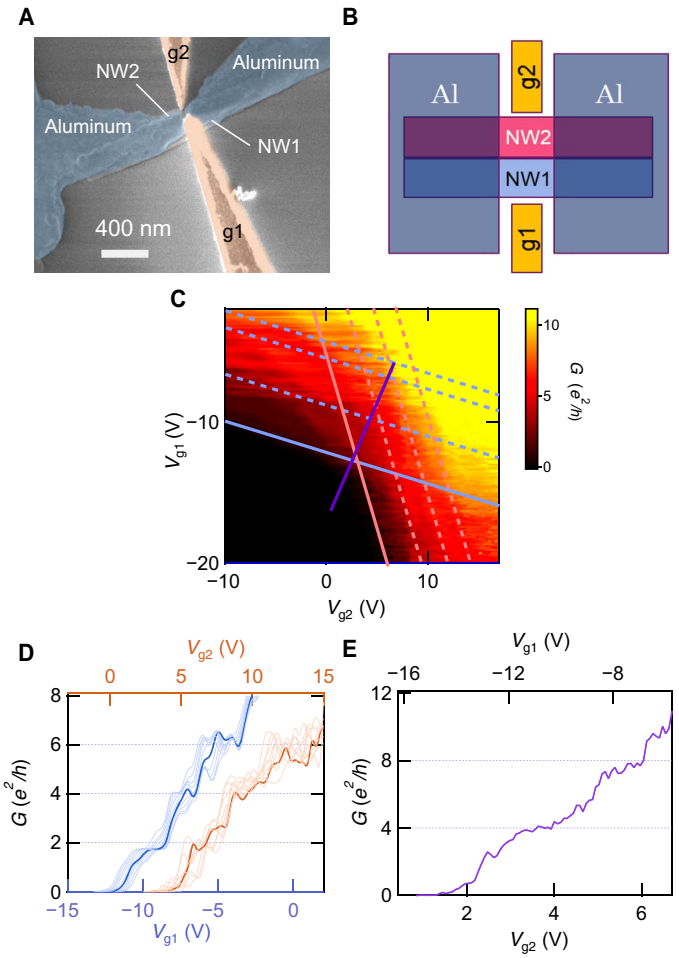

Fig. 1. Device structure and normal state conductance. (A) SEM image of the device. Two Al electrodes (blue) spaced by approximately 20 nm are placed on an InAs DNW. Two top gate electrodes (orange) spaced by approximately 80 nm are contacted to the DNW. Scale bar, 400 nm. (**B**) Schematic image of the device. NW1 and NW2 are mainly gated by electrode g1 with voltage V_{g1} and electrode g2 with voltage V_{g2}, respectively. (**C**) Differential conductance G in units of e^2/h as a function of V_{g1} and V_{g2} measured for magnetic field B = 250 mT and 50 mK. The blue (red) solid line follows the NW1 (NW2) pinch-off points. The dashed lines parallel to the solid lines indicate transitions between the respective NW plateaus [see (D)]. (**D**) G against V_{g1} (blue) was measured by setting V_{g2} between −5.0 and −8.0 V, where NW2 is pinched off, and G against V_{g2} (red) was measured by setting V_{g1} between −17.0 and −20.0 V, where NW1 is pinched off. All conductance curves show plateau-like features at 2, 4, and 6 e^2/h, as shown by the bold curves. (**E**) G plotted along the purple solid line in (C), where both NWs are equally populated. The conductance shows plateaus of 4 and 8 e^2/h when both NWs have two and four propagating channels, respectively.

Supercurrent in the DNW Josephson junction

Next, we measured the differential resistance R against bias current I under the magnetic field B = 0 T to observe the supercurrent. Figure 2 (A and C) shows typical results measured in (2,0), (4,0), and (6,0) of the NW1 region and in (0,2), (0,4), and (0,6) of the NW2 region, respectively. For sweeping the current from positive to negative, R becomes almost zero in the finite current range centered at I = 0 A, which indicates a supercurrent flowing through NW1 or NW2, and then abruptly increases and comes to a peak. We determine I_{sw} at the peak position. Almost the same I_{sw} is derived from the peak in the positive current region. We measured I_{sw} at several points on the same plateaus and took the average (see note S4 and fig. S5). The I_{sw} against G plots shown in Fig. 2 (A and C) are plotted in Fig. 2 (B and D), respectively. I_{sw} monotonically increases with G. Here, we use the G shown in Fig. 1C. We note that the Josephson junction is ballistic. This is supported by the normal conductance results, as discussed above, and the observed multiple Andreev reflection (see note S3 and fig. S4).

Next, we measured R against I in (2,2), (4,2), (6,2), (2,4), (2,6), and (4,4) of the DNW regions to study the CPS contributions. Figure 3A shows a typical result obtained in (2,2) (black), together with typical results in (2,0) and (0,2) (blue and red, respectively). Similarly, Fig. 3B shows the result in (4,4) (black), together with typical results in (4,0) and (0,4) (blue and red, respectively). The derived $I_{sw}(2,2)$ = 11.3 nA is much larger than $I_{sw}(2,0) + I_{sw}(0,2)$ = 4.78 nA. Here, $I_{sw}(m, n)$ and $G(m, n)$ are I_{sw} and G, respectively, measured in the (m, n) regions. Figure 3C shows a plot of $I_{sw}(m, n)$ against $G(m, n)$ in the DNW region (purple triangles) and $I_{sw}(m, 0) + I_{sw}(0, n)$ against $G(m, 0) + G(0, n)$ for the sum of I_{sw} measured in the respective NW regions (pink circles). $I_{sw}(m, n)$ is explicitly larger than $I_{sw}(m, 0) + I_{sw}(0, n)$ for all values of m and n.

The switching current I_{sw} for the respective NWs is the contribution from the LPT to the supercurrent. On the other hand, the CPS contribution, which only appears when both NWs have finite propagating channels, is observed as the surplus I_{sw} for the DNW compared to the sum of I_{sw} measured for the respective NWs. This evaluation method of CPS and LPT has been used in studies of CPS of double quantum dots coupled to a superconductor (*1*, *13*, *36*). Therefore, it can be concluded from the large I_{sw} enhancement in the DNW regions shown in Fig. 3C that there are significant CPS contributions. This CPS contribution is described as supercurrent, coherently carried by the split electrons in the DNW regions from one Al contact, which are recombined into a Cooper pair at another Al contact. We note that our device has no quantum dots, and the observed large CPS does not originate from the electrostatic energy in the dots, as reported previously.

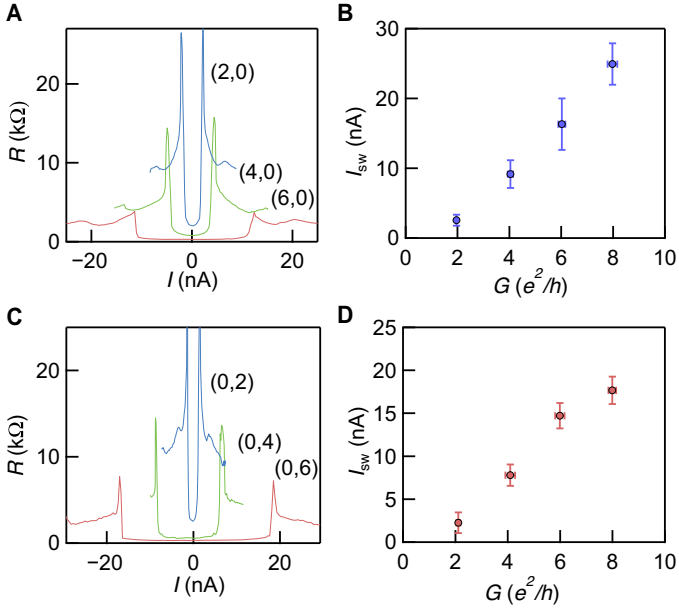

Fig. 2. Supercurrent due to LPT into each NW. (**A**) Typical differential resistance R against bias current I at B = 0 T measured in the conductance plateau regions of (2,0), (4,0), and (6,0), respectively, as shown in Fig. 1D. The supercurrent flows in the Josephson junction in the region of $R \simeq 0\ \Omega$. I_{sw} is evaluated from the peak position. (**B**) I_{sw} against G derived from measurement results shown in (A). The bars indicate variations of I_{sw} and G in the measurement performed at various points of the respective plateaus. I_{sw} monotonically depends on G. (**C** and **D**) Identical plots to (A) and (B), respectively, but for the conductance plateau regions of (0,2), (0,4), and (0,6).

DISCUSSION

CPS efficiency

From the I_{sw} results, we evaluated the CPS efficiency η defined by

$$\eta(m,n) = \frac{I_{sw}(m,n) - (I_{sw}(m,0) + I_{sw}(0,n))}{I_{sw}(m,n)} \times 100\%$$

The calculated values of $\eta(m, n)$ are summarized in Fig. 4A: 57.3, 31.6, 27.8, 48.8, 41.7, and 47.4% for the (2,2), (4,2), (6,2), (2,4), (2,6), and (4,4) regions, respectively. In particular, η(2,2) exceeds 50%, indicating that CPS, rather than LPT, is dominant in the supercurrent flowing through the DNW. Here, we measured the supercurrent in the Josephson junction; therefore, the two split electrons in the measured CPS component should maintain the singlet pairing phase coherence, and no contribution from quasiparticle tunneling is included in the results because I_{sw} is unaffected by quasiparticle tunneling.

As a result, η > 50% is obtained for (2,2). This result indicates that the LPT is significantly suppressed because if no e-e interaction is present in either NW, there is no suppression of the LPT, resulting in η ≤ 50%. This property is also found in the theoretical model of CPS in a junction of a superconductor and a double TLL (*5*). In this model, no e-e interaction represented as the TLL parameter K_c = 1 gives η ≤ 50% because there is no priority between the CPS and LPT. On the other hand, in the case of a finite e-e interaction in each NW with K_c < 1, the LPT is at a significant disadvantage to the CPS.

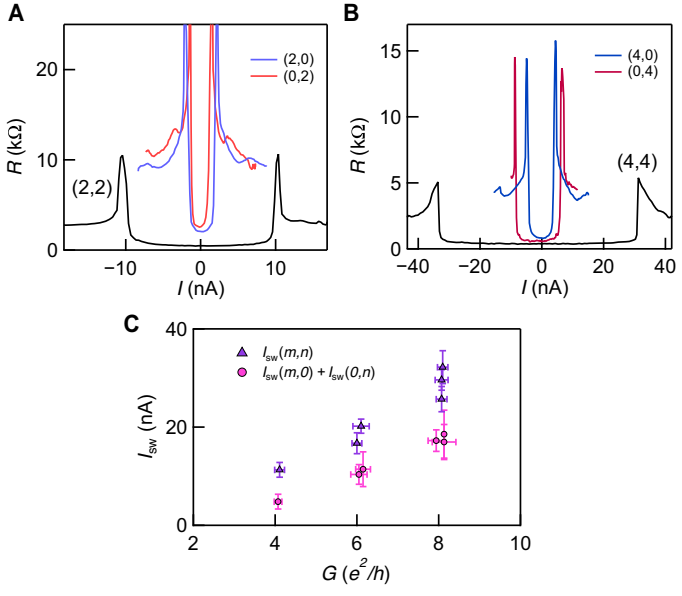

Fig. 3. Supercurrents in various conductance plateau regions. (**A**) Differential resistance R against I in the conductance plateau regions of (2,0), (0,2), and (2,2). I_{sw} in the (2,2) region is much larger than the sum of the I_{sw} values in the (2,0) and (0,2) regions. (**B**) R against I in the conductance plateau regions of (4,0), (0,4), and (4,4). The sum of the I_{sw} value in the (4,4) region is much larger than the sum of the I_{sw} values in the (4,0) and (0,4) regions. (**C**) $I_{sw}(m, n)$ against $G(m, n)$ in the conductance plateau regions (m, n) = (2,2), (2,4), (4,2), (2,6), (6,2), and (4,4), respectively, and the sum of $I_{sw}(m, 0)$ and $I_{sw}(0, n)$ against the sum of $G(0, n)$ and $G(m, 0)$ in the conductance plateau regions $(0, n)$ = (0,2) and (0,4) and $(m, 0)$ = (2,0) and (4,0). The bars indicate variations of I_{sw} and G in the measurement performed at various points of the respective plateaus. $I_{sw}(m, n)$ is significantly larger than $I_{sw}(n, 0) + I_{sw}(0, m)$ because of the CPS contribution to the DNW.

Our result of η(2,2) = 57.3% means that e-e interactions are of importance in the mechanism of the observed CPS. We note that the stronger spatial confinement originated from the small effective electron mass in InAs wires is beneficial for the stronger 1D e-e interaction (a smaller value of K_c) (*37*).

In Fig. 4A, we recognize two additional important features. First, η is asymmetric with respect to *m* and *n*, i.e., η(4,2) < η(2,4) and η(6,2) < η(2,6), although the normal-state conductance *G* is the same. In addition, the first feature is assigned to the asymmetry of the carrier density between the two NWs in the proximity region. In the device photograph in Fig. 1A, we see that NW1 is fully covered by the Al electrodes, but NW2 is not; therefore, the NW1 proximity region can have larger carrier density than the NW2 proximity region. The NW1 pinched-off voltage at V_{g2} = 0 V is $V_{g1} \simeq -12$ V, whereas that of NW2 at V_{g1} = 0 V is $V_{g2} \simeq -2$ V. In the theoretical model (*5*), lower carrier density in the NWs gives smaller K_c in the TLL case, which means stronger e-e interaction compared to the kinetic energy (*38*), so a larger η is expected. The stronger e-e interaction and a more significant LPT suppression expected in NW2 over NW1 could be the reason for the asymmetry of η(4,2) < η(2,4) and η(6,2) < η(2,6).

The second feature is that η decreases with increased NW channels. This feature is also assigned to the weaker e-e interaction in higher carrier density in the respective NWs because smaller η is obtained for plateaus associated with more channels. Here, we assume that the e-e interaction in the NWs varies with V_{g1} and V_{g2} to be biased toward the NWs located between the two Al electrodes. However, the NW length defined by the Al electrode gap is 20 nm, which is comparable to the Fermi wavelength and may be too short to significantly affect the interaction strength. We assign this contradiction to a broad potential landscape along the NWs across the boundary with the Al metal. Thus, the electrostatic potential of the gated NW gradually changes to that of the proximity region over a distance much longer than the Fermi wavelength. Then, the carrier density and therefore the e-e interaction are tuned by V_{g1} and V_{g2}. Two electrons that split from a Cooper pair in that proximity region propagate through the DNW, generating the CPS supercurrent. Hence, the large/small relation of the CPS and LPT, namely, η, changes with V_{g1} and V_{g2}, as expected when the 1D e-e interaction is gate-tuned.

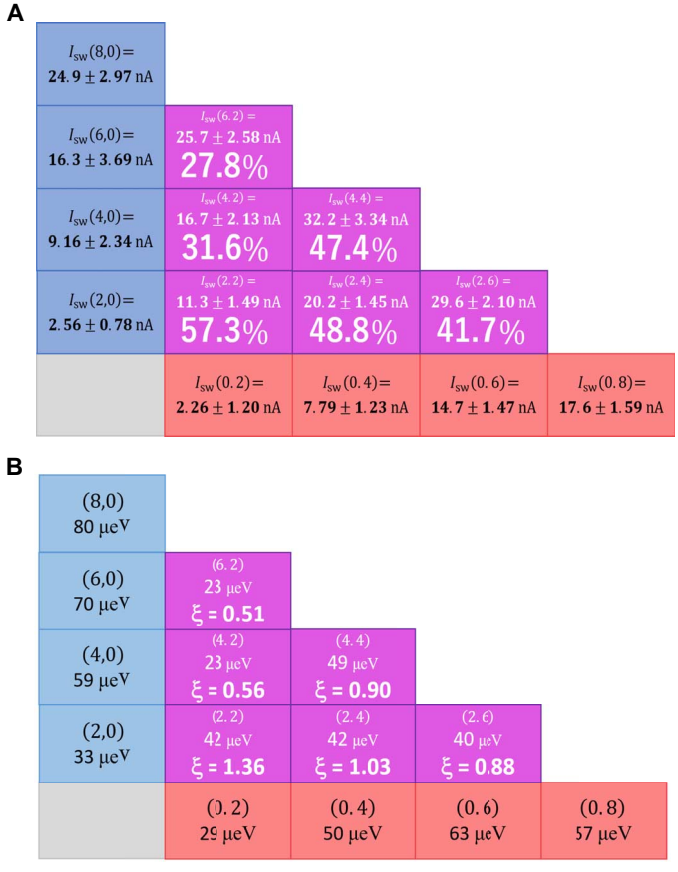

Fig. 4. CPS efficiency and gap energies of the interwire and intrawire superconductivity. (**A**) Schematic table of I_{sw} and CPS efficiency η obtained for various *m* and *n* values. I_{sw} enhancement due to CPS is observed for all conductance plateaus in the DNW regions. The CPS η is significantly larger than 50% in the (2,2) region. (**B**) Estimated superconducting gap energies and the ratio of the interwire and intrawire superconductivity ξ in the respective (*m*, *n*) regions. ξ is larger than unity in the (2,2) and (2,4) regions.

Gap energy of proximity-induced superconductivity via CPS and LPT

It is important to determine which of the contributions to the proximity-induced superconductivity (CPS or LPT) is larger in terms of the superconducting gap energy. We define $\xi(m,n) = \Delta_{CPS}(m,n)/\sqrt{\Delta_{NW1}(m,0)\Delta_{NW2}(0,n)}$ to discuss the CPS and LPT contributions, namely, the interwire and intrawire superconductivity. $\Delta_{CPS}(m,n)$, $\Delta_{NW1}(m,0)$, and $\Delta_{NW2}(0,n)$ are the superconducting gap energies of the interwire superconductivity via CPS, the intrawire superconductivity via LPT in NW1, and that in NW2, respectively. ξ is the gap energy ratio between the interwire and intrawire superconductivities; it is a measure for characterizing topological transition in DNW. The condition of ξ > 1 should be satisfied for the realization of Majorana Kramers pairs in DNWs with no magnetic field (*21*, *23*).

In the short ballistic Josephson junction with normal resistance R_n, $R_n I_{sw} = \pi\Delta/e$ with a superconducting gap energy of Δ and elementary charge of *e* (*39*, *40*). As shown in Fig. 1 (C to E), the present junction is in the ballistic regime. Thus, $\Delta_{CPS}(m,n)$, $\Delta_{NW1}(m,0)$, and $\Delta_{NW2}(0,n)$ can be approximately estimated as $G(m,n)^{-1}(I_{sw}(m,n) - I_{sw}(m,0) - I_{sw}(0,n))$, $G(m,0)^{-1}I_{sw}(m,0)$, and $G(0,n)^{-1}I_{sw}(0,n)$,

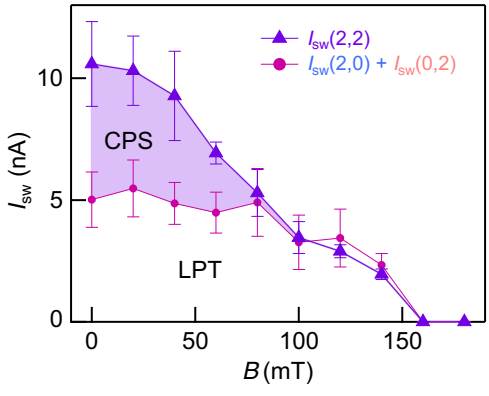

Fig. 5. Magnetic field dependence of CPS and LPT components. $I_{sw}(2,2)$ and $I_{sw}(2,0) + I_{sw}(0,2)$ measured at various magnetic fields of *B* = 0 to 180 mT. $I_{sw}(2,2)$ arises from both LPT into separate NWs and CPS into both NWs. The purple-shaded region corresponds to the I_{sw} enhancement due to CPS. The CPS component gradually decreases and vanishes at *B* = 80 mT, whereas the LPT component is unchanged up to *B* = 80 mT and then decreases down to I_{sw} = 0 nA at *B* = 160 mT.

respectively. The estimated values of Δ_{NW1}, Δ_{NW2}, Δ_{CPS}, and ξ are summarized in Fig. 4B. As m or n decreases, $\Delta_{NW1}(m, 0)$ and $\Delta_{NW2}(0, n)$ decrease. This behavior is consistent with our assumption that LPT is more strongly suppressed for the narrower channel because of the stronger e-e interaction, as discussed above. On the other hand, Δ_{CPS} does not change much; therefore, ξ is larger for the narrower channel. As a result, we find ξ larger than unity for (2,2) and (2,4). Therefore, the necessary condition for topological transition (*20*, *21*) is satisfied in our DNW junction.

Magnetic field dependence

Last, we studied the magnetic field dependence of the CPS. Figure 5 shows $I_{sw}(2,2)$ and $I_{sw}(2,0) + I_{sw}(0,2)$ measured under various magnetic fields. It is apparent that $I_{sw}(2,2)$ gradually decreases as the field initially increases up to B = 80 mT, whereas $I_{sw}(2,0) + I_{sw}(0,2)$ is almost unchanged. They become almost identical at B = 80 mT and then gradually decrease to zero in the same manner as the field increases up to 160 mT. This indicates that both $I_{sw}(2,2)$ and $I_{sw}(2,0) + I_{sw}(0,2)$ only depend on LPT in NW1 and NW2 for 80 mT $\leq B \leq$ 160 mT. Therefore, the CPS contribution is only present in the range of B = 0 to 80 mT, as indicated by the purple-shaded area, whereas the LPT contribution remains substantial. Note that essentially identical behavior is observed for $I_{sw}(4,4)$ and $I_{sw}(4,0) + I_{sw}(0,4)$, suggesting that the CPS mechanism is universal for 1D electron systems (see note S5 and fig. S6).

This peculiar magnetic field dependence is qualitatively explained by the critical field B_c of superconducting thin film, whose coherence length and penetration length are sufficiently longer than film thickness d (*41*, *42*). The theoretical indication of $B_c \approx 1/d$ means that the critical field becomes half when the film thickness becomes twice. This can be applied to a superconducting wire when the magnetic field is perpendicular to the direction of the wire. As a result, when the Cooper pair spreads over both NWs in the CPS contribution, the critical field becomes half compared with that for the LPT contribution, in which the Cooper pairs are localized in either of the NWs. Therefore, the magnetic field dependence observed for $I_{sw}(2,2)$ and $I_{sw}(2,0) + I_{sw}(0,2)$ supports the idea that the enhancement in $I_{sw}(2,2)$ originates from the CPS, such that the two electrons of the Cooper pair split into two NWs.

CONCLUSION

In summary, we examined CPS and LPT in a ballistic InAs DNW using a Josephson junction. We observed a large CPS efficiency for the DNW due to suppression of LPT into the respective NWs resulting from 1D e-e interaction. The CPS efficiency is tunable by adjusting the gate voltages and can well exceed 50% for narrow NW channels. In addition, the interwire superconducting gap is greater than the intrawire one when each NW has a single channel. These results suggest that the InAs DNW coupled to a superconductor can hold time-reversal invariant topological superconductivity and Majorana Kramers pairs at the edges with no magnetic field. Our results pave the way for the utilization of 1D e-e interaction to reveal the physics of high-efficiency CPS and to engineer MFs in DNW systems coupled to a superconductor via CPS.

MATERIALS AND METHODS

The InAs NWs have a diameter of approximately 80 nm and were grown by chemical beam epitaxy. We transferred the NWs on the growth substrate onto an Si substrate covered by a 280-nm-thick SiO_2 film and selected closely spaced parallel DNWs to make Al-DNW-Al junctions. We made a polymethyl methacrylate pattern of the Al electrodes using electron beam lithography and performed a NW surface treatment before evaporating Ti (1 nm)/Al (100 nm): reactive ion etching to remove the polymethyl methacrylate residue and sulfur passivation to remove the surface oxide (see note S1 and figs. S1 and S2). For the fabrication of the gate structure, we grew a 40-nm-thick Al_2O_3 layer by atomic layer deposition and fabricated the gate electrodes of Ti (5 nm)/Au (150 nm).

SUPPLEMENTARY MATERIALS

Supplementary material for this article is available at http://advances.sciencemag.org/cgi/content/full/5/10/eaaw2194/DC1

Fig. S1. Atomic force microscopy images of the nanowires before deposition of Al contact electrodes.
Fig. S2. SEM image of a device similar to the one measured but before depositing the top gate electrodes.
Fig. S3. Differential conductance (G) properties of the Al-InAs DNW-Al junction device.
Fig. S4. Differential conductance G against V_{sd} measured at B = 0 T for a bias point on the respective plateau of (m, n).
Fig. S5. Gate bias points set for supercurrent measurement at B = 0 T indicated on the surface plot of G against V_{g1} and V_{g2} at B = 250 mT.
Fig. S6. Magnetic field dependence of $I_{sw}(m, n)$ and $I_{sw}(m, 0) + I_{sw}(0, n)$ measured at various quantized conductance plateaus with m and n.
Fig. S7. $I_{sw}(m, 0) + I_{sw}(0, n)$ against $G(m, 0) + G(0, n)$ measured at B = 80 mT and B = 120 mT.
Fig. S8. $I_{sw}(2,2)$ as a function of temperature.
Note S1. Details of fabrication process for the DNW Josephson junctions
Note S2. Magnetic field dependence of the superconducting gap
Note S3. Multiple Andreev reflection and quantized conductance outside the superconducting gap
Note S4. Measurement points for supercurrent
Note S5. Magnetic field dependence of CPS and LPT
Note S6. Another possible mechanism for the I_{sw} enhancement
Note S7. Joule heating
References (*43*–*50*)

REFERENCES AND NOTES

1. P. Recher, E. V. Sukhorukov, D. Loss, Andreev tunneling, Coulomb blockade, and resonant transport of nonlocal spin-entangled electrons. *Phys. Rev. B* **63**, 165314 (2001).
2. G. B. Lesovik, T. Martin, G. Blatter, Electronic entanglement in the vicinity of a superconductor. *Eur. Phys. J. B Condens. Matter Complex Syst.* **24**, 287–290 (2001).
3. V. Bouchiat, N. Chtchelkatchev, D. Feinberg, G. B. Lesovik, T. Martin, J. Torrès, Single-walled carbon nanotube-superconductor entangler: Noise correlations and Einstein-Podolsky-Rosen states. *Nanotechnology* **14**, 77 (2002).
4. C. Bena, S. Vishveshwara, L. Balents, M. P. A. Fisher, Quantum entanglement in carbon nanotubes. *Phys. Rev. Lett.* **89**, 037901 (2002).
5. P. Recher, D. Loss, Superconductor coupled to two Luttinger liquids as an entangler for electron spins. *Phys. Rev. B* **65**, 165327 (2002).
6. N. M. Chtchelkatchev, G. Blatter, G. B. Lesovik, T. Martin, Bell inequalities and entanglement in solid-state devices. *Phys. Rev. B* **66**, 161320 (2002).
7. P. Burset, W. J. Herrera, A. L. Yeyati, Microscopic theory of Cooper pair beam splitters based on carbon nanotubes. *Phys. Rev. B* **84**, 115448 (2011).
8. L. Hofstetter, S. Csonka, J. Nygård, C. Schönenberger, Cooper pair splitter realized in a two-quantum-dot Y-junction. *Nature* **461**, 960–963 (2009).
9. L. G. Herrmann, F. Portier, P. Roche, A. Levy Yeyati, T. Kontos, C. Strunk, Carbon nanotubes as cooper-pair beam splitters. *Phys. Rev. Lett.* **104**, 026801 (2010).
10. J. Schindele, A. Baumgartner, C. Schönenberger, Near-unity cooper pair splitting efficiency. *Phys. Rev. Lett.* **109**, 157002 (2012).
11. A. Das, Y. Ronen, M. Heiblum, D. Mahalu, A. V. Kretinin, H. Shtrikman, High-efficiency Cooper pair splitting demonstrated by two-particle conductance resonance and positive noise cross-correlation. *Nat. Commun.* **3**, 1165 (2012).
12. Z. B. Tan, D. Cox, T. Nieminen, P. Lähteenmäki, D. Golubev, G. B. Lesovik, P. J. Hakonen, Cooper pair splitting by means of graphene quantum dots. *Phys. Rev. Lett.* **114**, 096602 (2015).
13. R. S. Deacon, A. Oiwa, J. Sailer, S. Baba, Y. Kanai, K. Shibata, K. Hirakawa, S. Tarucha, Cooper pair splitting in parallel quantum dot Josephson junctions. *Nat. Commun.* **6**, 7446 (2015).

14. G. Fülöp, F. Domínguez, S. d'Hollosy, A. Baumgartner, P. Makk, M. H. Madsen, V. A. Guzenko, J. Nygård, C. Schönenberger, A. Levy Yeyati, S. Csonka, Magnetic field tuning and quantum interference in a Cooper pair splitter. *Phys. Rev. Lett.* **115**, 227003 (2015).
15. I. V. Borzenets, Y. Shimazaki, G. F. Jones, M. F. Craciun, S. Russo, M. Yamamoto, S. Tarucha, High efficiency CVD graphene-lead (Pb) cooper pair splitter. *Sci. Rep.* **6**, 23051 (2016).
16. S. Baba, C. Jünger, S. Matsuo, A. Baumgartner, Y. Sato, H. Kamata, K. Li, S. Jeppesen, L. Samuelson, H. Q. Xu, C. Schönenberger, S. Tarucha, Cooper-pair splitting in two parallel InAs nanowires. *New J. Phys.* **20**, 063021 (2018).
17. B. Braunecker, P. Burset, A. Levy Yeyati, Entanglement detection from conductance measurements in carbon nanotube Cooper pair splitters. *Phys. Rev. Lett.* **111**, 136806 (2013).
18. S.-i. Tomonaga, Remarks on Bloch's method of sound waves applied to many-fermion problems. *Prog. Theor. Phys.* **5**, 544–569 (1950).
19. J. M. Luttinger, An exactly soluble model of a many-Fermion system. *J. Math. Phys.* **4**, 1154 (1963).
20. J. Klinovaja, D. Loss, Parafermions in an interacting nanowire bundle. *Phys. Rev. Lett.* **112**, 246403 (2014).
21. J. Klinovaja, D. Loss, Time-reversal invariant parafermions in interacting Rashba nanowires. *Phys. Rev. B* **90**, 045118 (2014).
22. H. Ebisu, B. Lu, J. Klinovaja, Y. Tanaka, Theory of time-reversal topological superconductivity in double Rashba wires: Symmetries of Cooper pairs and Andreev bound states. *Prog. Theor. Exp. Phys.* **2016**, 083I01 (2016).
23. C. Schrade, M. Thakurathi, C. Reeg, S. Hoffman, J. Klinovaja, D. Loss, Low-field topological threshold in Majorana double nanowires. *Phys. Rev. B* **96**, 035306 (2017).
24. C. Reeg, C. Schrade, J. Klinovaja, D. Loss, DIII topological superconductivity with emergent time-reversal symmetry. *Phys. Rev. B* **96**, 161407 (2017).
25. A. Y. Kitaev, Unpaired Majorana fermions in quantum wires. *Phys. Uspekhi* **44**, 131 (2001).
26. V. Mourik, K. Zuo, S. M. Frolov, S. R. Plissard, E. P. A. M. Bakkers, L. P. Kouwenhoven, Signatures of Majorana fermions in hybrid superconductor-semiconductor nanowire devices. *Science* **336**, 1003–1007 (2012).
27. L. P. Rokhinson, X. Liu, J. K. Furdyna, The fractional a.c. Josephson effect in a semiconductor–superconductor nanowire as a signature of Majorana particles. *Nat. Phys.* **8**, 795–799 (2012).
28. M. T. Deng, C. L. Yu, G. Y. Huang, M. Larsson, P. Caroff, H. Q. Xu, Anomalous zero-bias conductance peak in a Nb–InSb nanowire–Nb hybrid device. *Nano Lett.* **12**, 6414–6419 (2012).
29. A. Das, Y. Ronen, Y. Most, Y. Oreg, M. Heiblum, H. Shtrikman, Zero-bias peaks and splitting in an Al–InAs nanowire topological superconductor as a signature of Majorana fermions. *Nat. Phys.* **8**, 887–895 (2012).
30. M. T. Deng, C. L. Yu, G. Y. Huang, M. Larsson, P. Caroff, H. Q. Xu, Parity independence of the zero-bias conductance peak in a nanowire based topological superconductor-quantum dot hybrid device. *Sci. Rep.* **4**, 7261 (2014).
31. S. M. Albrecht, A. P. Higginbotham, M. Madsen, F. Kuemmeth, T. S. Jespersen, J. Nygård, P. Krogstrup, C. M. Marcus, Exponential protection of zero modes in Majorana islands. *Nature* **531**, 206–209 (2016).
32. D. Rainis, D. Loss, Majorana qubit decoherence by quasiparticle poisoning. *Phys. Rev. B* **85**, 174533 (2012).
33. D. J. Clarke, J. Alicea, K. Shtengel, Exotic non-Abelian anyons from conventional fractional quantum Hall states. *Nat. Commun.* **4**, 1348 (2013).
34. R. S. K. Mong, D. J. Clarke, J. Alicea, N. H. Lindner, P. Fendley, C. Nayak, Y. Oreg, A. Stern, E. Berg, K. Shtengel, M. P. A. Fisher, Universal topological quantum computation from a superconductor-Abelian quantum hall heterostructure. *Phys. Rev. X* **4**, 011036 (2014).
35. D. J. Clarke, J. Alicea, K. Shtengel, Exotic circuit elements from zero-modes in hybrid superconductor–quantum-Hall systems. *Nat. Phys.* **10**, 877–882 (2014).
36. S. Baba, J. Sailer, R. S. Deacon, A. Oiwa, K. Shibata, K. Hirakawa, S. Tarucha, Superconducting transport in single and parallel double InAs quantum dot Josephson junctions with Nb-based superconducting electrodes. *Appl. Phys. Lett.* **107**, 222602 (2015).
37. Y. Sato, S. Matsuo, C. H. Hsu, P. Stano, K. Ueda, Y. Takeshige, H. Kamata, J. S. Lee, B. Shojaei, K. Wickramasinghe, J. Shabani, C. Palmstrøm, Y. Tokura, D. Loss, S. Tarucha, Strong electron-electron interactions of a Tomonaga-Luttinger liquid observed in InAs quantum wires. *Phys. Rev. B* **99**, 155304 (2019).
38. C. L. Kane, M. P. A. Fisher, Transport in a one-channel Luttinger liquid. *Phys. Rev. Lett.* **68**, 1220 (1992).
39. C. W. J. Beenakker, H. van Houten, Josephson current through a superconducting quantum point contact shorter than the coherence length. *Phys. Rev. Lett.* **66**, 3056 (1991).
40. A. Furusaki, H. Takayanagi, M. Tsukada, Josephson effect of the superconducting quantum point contact. *Phys. Rev. B* **45**, 10563 (1992).
41. V. L. Ginzburg, L. D. Landau, On the Theory of superconductivity. *Zh. Eksp. Teor. Fiz.* **20**, 1064–1082 (1950).
42. F. E. Harper, M. Tinkham, The mixed state in superconducting thin films. *Phys. Rev.* **172**, 441 (1968).
43. Y.-J. Doh, J. A. van Dam, A. L. Roset, E. P. A. M. Bakkers, L. P. Kouwenhoven, S. De Franceschi, Tunable supercurrent through semiconductor nanowires. *Science* **309**, 272–275 (2005).
44. J. A. Van Dam, Y. V. Nazarov, E. P. A. M. Bakkers, S. De Franceschi, L. P. Kouwenhoven, Supercurrent reversal in quantum dots. *Nature* **442**, 667–670 (2006).
45. W. Chang, S. M. Albrecht, T. S. Jespersen, F. Kuemmeth, P. Krogstrup, J. Nygård, C. M. Marcus, Hard gap in epitaxial semiconductor–superconductor nanowires. *Nat. Nanotechnol.* **10**, 232–236 (2015).
46. H. A. Nilsson, P. Samuelsson, P. Caroff, H. Q. Xu, Supercurrent and multiple andreev reflections in an InSb nanowire josephson junction. *Nano Lett.* **12**, 228–233 (2012).
47. P. Jarillo-Herrero, J. A. van Dam, L. P. Kouwenhoven, Quantum supercurrent transistors in carbon nanotubes. *Nature* **439**, 953–956 (2006).
48. H. Grabert, U. Weiss, Crossover from thermal hopping to quantum tunneling. *Phys. Rev. Lett.* **53**, 1787 (1984).
49. V. Ambegaokar, B. I. Halperin, Voltage due to thermal noise in the dc Josephson effect. *Phys. Rev. Lett.* **22**, 1364 (1969).
50. S. Roddaro, A. Pescaglini, D. Ercolani, L. Sorba, F. Giazotto, F. Beltram, Hot-electron effects in InAs nanowire Josephson junctions. *Nano Res.* **4**, 259–265 (2011).

Acknowledgments: We thank P. Stano and C.-H. Hsu for fruitful discussion. **Funding:** This work was partially supported by a Grant-in-Aid for Scientific Research (B) (grant no. JP18H01813); a Grant-in-Aid for Young Scientific Research (A) (grant no. JP15H05407); a Grant-in-Aid for Scientific Research (A) (grant no. JP16H02204); a Grant-in-Aid for Scientific Research (S) (grant nos. JP26220710 and JP19H05610); JSPS Early-Career Scientists (grant no. JP18K13486); JSPS Program for Leading Graduate Schools (MERIT); JSPS Research Fellowship for Young Scientists (grant nos. JP19J13867, JP18J14172) from JSPS; a Grants-in-Aid for Scientific Research on Innovative Area Nano Spin Conversion Science (grant no. JP17H05177); a Grant-in-Aid for Scientific Research on Innovative Area Topological Materials Science (grant no. JP16H00984) from MEXT; JST CREST (grant no. JPMJCR15N2); JST PRESTO (grant no. JPMJPR18L8) the ImPACT Program of Council for Science, Technology, and Innovation (Cabinet Office, Government of Japan); the Ministry of Science and Technology of China (MOST) through the National Key Research and Development Program of China (grant nos. 2016YFA0300601 and 2017YFA0303304); the National Natural Science Foundation of China (grant nos. 91221202, 91421303, and 11874071); and the Swedish Research Council (VR). **Author contributions:** S.M. and S.T. conceived the experiments. K.L., S.J., L.S., and H.X. grew the NWs. K.U. fabricated the device, while S.M., S.B., H.K., Y.S., and Y.T. contributed to the fabrication. K.U. and S.M. executed the measurements. K.U., S.M., and S.T. analyzed and interpreted the data and wrote the paper. S.T. supervised the study. **Competing interests:** The authors declare that they have no competing interests. **Data and materials availability:** All data needed to evaluate the conclusions in the paper are present in the paper and/or the Supplementary Materials. Additional data related to this paper may be requested from the authors.

Submitted 30 November 2018
Accepted 8 September 2019
Published 4 October 2019
10.1126/sciadv.aaw2194

Citation: K. Ueda, S. Matsuo, H. Kamata, S. Baba, Y. Sato, Y. Takeshige, K. Li, S. Jeppesen, L. Samuelson, H. Xu, S. Tarucha, Dominant nonlocal superconducting proximity effect due to electron-electron interaction in a ballistic double nanowire. *Sci. Adv.* **5**, eaaw2194 (2019).